N 84 - 32 5 0 8

Microstructure and Surface Chemistry of Amorphous Alloys Important to Their Friction and Wear Behavior

Kazuhisa Miyoshi and Donald H. Buckley
Lewis Research Center
Cleveland, Ohio

NASA

MICROSTRUCTURE AND SURFACE CHEMISTRY OF AMORPHOUS ALLOYS
IMPORTANT TO THEIR FRICTION AND WEAR BEHAVIOR

Kazuhisa Miyoshi and Donald H. Buckley*

ABSTRACT

An investigation was conducted to examine the microstructure and surface chemistry of amorphous alloys, and their effects on tribological behavior.

The results indicate that the surface oxide layers present on amorphous alloys are effective in providing low friction and a protective film against wear in air. Clustering and crystallization in amorphous alloys can be enhanced as a result of plastic flow during the sliding process at a low sliding velocity and at room temperature. Clusters or crystallites with sizes to 150 nm and a diffused honeycomb-shaped structure are produced on the wear surface. Temperature effects lead to drastic changes in surface chemistry and friction behavior of the alloys at temperatures to $750°$ C. Contaminants can come from the bulk of the alloys to the surface upon heating and impart to the surface oxides at $350°$ C and boron nitride above $500°$ C. The oxides increase friction while the boron nitride reduces friction drastically in vacuum.

1. INTRODUCTION

Metallic glasses are currently finding increased application in the aerospace industry [1]. They are used for joining internal assemblies in gas turbines. Nickel-based brazed foils of the BNi class are replacing the more expensive gold-based BAu-4 foils in engine valves and many other components. However, like BAu-4, the nickel-based filler metals have excellent flow behavior, are compatible with most stainless steels and nickel alloys, and offer an outstanding combination of high-temperature strength, fatigue properties, and oxidation and corrosion resistance [1].

A combination of favorable mechanical and physical properties makes metallic glasses candidates for other technological applications. For example, the combination of high permeability and high hardness makes these materials suitable for use in highly developed magnetic recording devices (e.g., video tape recorders). In most high-density devices, a magnetic head in sliding contact with a magnetic tape is used for recording and playback. Therefore, the magnetic head and tape must have good wear resistance.

Metallic glasses can also be used in foil bearings. The highly disordered structures of metallic glass would be resistant to radiation damage, and, thus, have potential for use where constant mechanical properties are required under irradiation. The mechanical and physical properties of metallic glasses are, therefore, of basic scientific interest.

Metallic glasses have several properties that make them attractive for tribological applications. These properties include great adhesion, shear strength, impact penetration, corrosion resistance, stiffness, and ductility. Relatively little research, however, has been done on the friction, adhesive wear, and abrasive wear properties of the metallic glasses [2-7].

This paper is principally concerned with a fundamental understanding of microstructure and chemistry of amorphous alloy surfaces, and their effects on tribological properties (friction and wear). Sliding friction experiments were conducted with three ferrous-base amorphous alloy compositions in vacuum (30 nPa) and a laboratory air or argon atmosphere. A rider of aluminum oxide was made to slide on the amorphous alloy surfaces under loads of from 0.1 to 2.5 N and at sliding velocities of from 0.033 to 0.17 mm/sec. The vacuum experiments were conducted at temperatures of from room to $750°$ C.

*National Aeronautics and Space Administration, Lewis Research Center, Cleveland, Ohio 44135

2. MATERIALS

Three amorphous alloy compositions were examined in this investigation. The compositions and some of their properties are presented in table I. The alloys were foils (30 to 33 μm-thick ribbon), and were used in the as-cast condition. The spherical riders that were made to slide on the foil were single-crystal aluminum oxide (sapphire) spheres and the diameter of the spheres were 3.2 and 6.4 mm.

3. APPARATUSES

Two apparatuses were used in this investigation (Fig. 1). They both use a pin on flat configuration. One consists of an ultra-high vacuum system capable of measuring adhesion, load, and friction and contains an XPS spectrometer. Figure 1(a) indicates the major components, including the electron energy analyzer, the X-ray source, and the ion gun used for ion sputter etching. A manipulator-mounted beam was projected into a vacuum chamber. The beam contained two flats machined normal to each other with strain gages mounted thereon. The load was applied by moving the beam normal to the flat and was sensed by strain gages. The vertical sliding motion of the pin along the flat surface was accomplished through a motorized manipulator assembly. The friction force under an applied load was measured during vertical translation by a strain gage mounted normal to that used to measure load.

The second apparatus used in this investigation is shown schematically in Fig. 1(b). The pin was made to traverse a distance of 10 mm on the surface of the foil. Motion was reciprocal. The pin was loaded against the foil with dead weights. The arm retaining the rider contained strain gages to measure the tangential and normal forces. The entire apparatus was housed in a plastic box.

4. EXPERIMENTAL PROCEDURE

Specimen Preparation and Heating

The foil specimen was attached to an insulator flat with tantalum supporting sheets (Fig. 1). The specimen was directly in contact with the sheets. The flat and pin surfaces were rinsed with 200-proof ethyl alcohol just before they were placed in the vacuum chamber. After the specimens were placed in the vacuum chamber, the system was evacuated and then baked out at 250° C to obtain a pressure of 30 nPa (2×10^{-10} torr) or lower.

Both flat and pin specimens were argon ion sputter cleaned. Treatment was next conducted in situ, and this included heating to a maximum temperature of 750° C at a pressure of 600 nPa for 20 to 30 min. The foil was resistance heated. The temperature was measured with a type K (Ni-Cr versus Ni-Al) thermocouple in contact with the specimen.

Specimens were thinned for transmission electron microscopy and diffraction studies by ion-etching and electropolishing.

Surface Chemical Analysis

The foil surfaces were analyzed by X-ray photoelectron spectroscopy (XPS). The depth analysis with XPS is of the order of 2 to 3 nm, and the ultimate sensitivity is sufficient to allow fractions of a monolayer to be detected and identified. A magnesium K_α X-ray source was used with an X-ray source power of 400 W. All XPS analyses were conducted at room temperature.

Friction Experiments

In the ultra-high-vacuum system, in situ friction experiments were conducted with the surface-treated foil specimens over a temperature range of from room to 750° C. A load of 0.2 N was applied to the pin-flat contact by deflecting the beam, as shown in Fig. 1. To obtain consistent experimental conditions, contact before sliding was maintained for 30 sec. Both the load and friction force were continuously monitored during a friction experiment. Sliding velocity was 3 mm/min with a total sliding distance of 2 to 3 mm. All single-pass friction experiments were conducted in a 30 nPa vacuum. The coefficients of friction reported herein were obtained by averaging three to five measurements.

In argon or a laboratory air atmosphere the foils of the amorphous alloys and the pin specimen surfaces were scrubbed with levigated alumina, rinsed with tap water and then with distilled water, and finally rinsed with ethyl alcohol. After the surface was dried with argon gas, the specimens were placed into the experimental apparatus. The specimen surfaces were then brought into contact and loaded, and the friction experiment was begun.

5. RESULTS AND DISCUSSION

Amorphous Alloy Surfaces

To establish the exact crystalline state of the amorphous alloy surfaces, microstructure was examined by transmission electron

microscopy and diffraction in a microscope operating at 100 kV.

A typical example of the structure of the as-received amorphous alloy foil is shown in Fig. 2. The amorphous alloy lacks the macroscopic structural features common in crystalline metals. In the absence of macroscopic crystallinity, neither grains, grain boundaries, grain orientations nor additional phases exist. However, black spots, which are believed to be nuclei and/or crystallites with a size range to 4 nm, are apparent in the photomicrograph. Very diffused honeycomb-shaped structures formed by dark grey bands as a result of segregation and clustering of transition metals and metalloids are also apparent in the photomicrograph.

The electron diffraction pattern for the as-received foil presented in Fig. 2 indicates that the amorphous alloy foil was not completely amorphous but contained extremely small nuclei and/or clusters of approximately a few nanometers in size.

All the XPS spectra taken from the surfaces of three amorphous alloys as received clearly revealed adsorbed oxygen and carbon contaminants in addition to the various alloying constituents of the nominal bulk composition. Beneath this layer of adsorbate there is a mixture layer of oxides of the alloying constituents.

Fe_{2p} peaks of the as-received $Fe_{67}Co_{18}B_{14}Si_1$ specimen are shown as an example in Fig. 3. The spectrum for the surface before cleaning clearly indicates that there were iron oxides such as Fe_2O_3 on the foil surface. The spectra taken after the foil surface had been argon sputter cleaned for 2 and 4 min reveal that the lines for Fe_{2p} were split asymmetrically into doublet peaks. The doublet peaks are associated with iron oxides and iron. The spectra taken after the foil surface had been argon sputter cleaned for 60 min clearly indicate the Fe_{2p} peaks associated with iron, while the iron oxide peak is very small. The results at 30 min sputtering were similar to those at 60 min.

The as-received $Fe_{67}Co_{18}B_{14}Si_1$ foil contained the oxides of cobalt, boron and silicon as well [2]. The oxide layers are extremely important for amorphous alloys from a tribological point of view, because it is very hard and tenaciously bonded to the alloying constituents. This can provide good wear resistance, and will be discussed in the following section.

The XPS spectra of the surface argon sputtered for 60 min contained small amounts of carbide and oxide contaminants such as silicon carbide and silicon dioxide, although

the $Fe_{67}Co_{18}B_{14}Si_1$ foil was not supposed to contain carbon and oxygen. The contaminants (i.e., oxygen and carbon) may be introduced from the environment into the bulk of the alloy and form bulk contaminants, such as carbides and oxides, in the alloy during the casting process.

The argon-ion-sputter cleaned surface conditions of the three amorphous alloy foils analyzed by XPS are summarized in table II. The relative concentrations of the various constituents on the surfaces were different from the nominal compositions.

Friction and Wear

Sliding friction experiments were conducted with the three as-received amorphous alloys, where normal residual oxides were present on the surface, and in contact with an aluminum oxide ball in argon or in laboratory air. Comparative experiments were made with practical materials such as 304 stainless steel foil and 440C stainless steel. The 304 stainless steel was of equivalent foil thickness as the amorphous alloys.

When the amorphous alloys were rubbed by the 6.4 mm-diameter and 3.2 mm-diameter aluminum oxide riders at a load of 2.5 N (providing contact pressure of approximately 0.8 and 1.3 GPa, respectively) for 30 min, essentially no detectable wear existed on the surface of the three amorphous alloys. There was a complete absence of any visible wear track when examined by the optical and scanning electron microscope.

Wear tracks were, however, visible on the 304 stainless steel foil and the 440C stainless steel. The wear damage of 440C stainless steel was much less than that of 304 stainless steel. A copious amount of wear debris was generated and considerable plastic flow and wear occurred to the 304 stainless steel surface, and clumps of metal appeared in the wear track [8].

Thus, surface oxide layers present in the amorphous alloys were very effective in providing a protective film against wear.

Since no visible wear was observed on the amorphous alloys, sliding friction experiments were conducted with the 3.2 mm-diameter aluminum oxide rider at a load of 2.5 N and with the sliding time extended to 150 hr in order to provide more severe conditions and to remove the protective oxide films.

Figure 4 presents scanning electron micrographs of typical wear tracks on the amorphous alloy $Fe_{67}Co_{18}B_{14}Si_1$ and the 304 stainless steel foil surfaces at a total sliding time of 5 hr. Oxide wear debris particles were generated on the amorphous

alloy surface, while metal wear debris particles were primarily generated on the stainless steel surface. With the amorphous alloy microscopic brittle fracture and breaking up of oxide layers took place, and fine oxide wear debris particles were mainly produced. With the 304 stainless steel, however, rupturing the bonds of cohesively weaker 304 stainless steel occurred, cavities were formed in the material, and then small platelet-type metallic wear debris particles were subsequently produced.

Figure 5 illustrates a detailed examination of the oxide wear debris (submicrons to microns in size) produced on the amorphous alloy as a result of the sliding action. The scanning electron micrographs clearly reveal powdery and whiskery (needle-shaped) oxide wear debris particles on and near the wear track after sliding contact with the aluminum oxide rider.

Figure 4(a) discussed above also clearly revealed that plastic flow occurred in the amorphous alloy. The sliding action resulted in plastic deformation not only in the wear track but also at the side of the wear track. Multiple shear deformation bands were observed on the side of the wear track (as shown in Fig. 4(a)). The plastic flow, observed on the side of the wear track, occurs in the form of highly localized shear deformation bands. Thus, a concentration of large shear strains develops in a band during sliding friction process. The shear bands are similar to those in crystalline metals [9].

Figure 6(a) clearly reveals that plastic flow occurs in the wear track of the amorphous alloy with repeated sliding.

When the aluminum oxide rider in sliding contact with the amorphous alloy was examined by the scanning electron microscope, there were flow films of the alloy adhered and transferred to the aluminum oxide rider surface (as shown in Fig. 6(b)).

During a 150-hr sliding period, considerable plastic flow occurred and considerable oxide debris was generated on the amorphous alloy. Figure 7 reveals evidence of wear damage and large particles of wear debris, which were generated at local spots. Shear fracture occurs at very local areas in the amorphous alloy during repeated sliding. The wear volume was 0.01 mm^3 or less. The wear rate, which is defined as the quantity of amorphous alloy removed under a unit load and with a unit distance of sliding, was 5×10^{-9} mm^3/Nmm.

Mechanical Effects

Crystallization of amorphous alloy in mechanical contact with an aluminum oxide rider (3.2 mm-radius) has been observed to occur during sliding friction with a relatively slow sliding velocity (1.5 mm/sec), wherein frictional heating is negligible.

A typical example of the wear surface of the $Fe_{67}Co_{18}B_{14}Si_1$ amorphous alloy run for 150 hr is shown in Fig. 8. Dark dots and bands, which are believed to be clusters or crystallites ranging in size from 10 to 50 nm, are apparent. Diffused honeycomb-shaped structures formed by dark grey bands are due to segregation and preferential clustering of transition metals and metalloids. The electron diffraction pattern also indicates that the wear surface contained small clusters or grains.

Figure 9 presents bright and dark field images and the diffraction pattern of a local area of the wear surface on the amorphous alloy. Dark spots, believed to be clusters or crystallites ranging in size to 150 nm, observed in the bright image are reversed in the dark image. The diffraction pattern was also taken from the spots. Figure 9 clearly indicates a partially crystallized phase in the matrix. As seen from these micrographs, star-shaped crystals grow in the $Fe_{67}Co_{18}B_{14}Si_1$ alloy.

The diffraction pattern includes spotting rings which lose their continuity at $360°$ and diffuse halos. The spotty ring is essentially that for a crystalline material and most of the spot pattern of the crystallized phase was identified as $\alpha-Fe_2O_3$.

The diffuse halos indicate that the matrix contains extremely small grains of approximately a few nanometers in size. The results suggest that crystallization may occur by nucleation and growth processes of $\alpha-Fe$. The dispersed and primary crystallized $\alpha-Fe$ phase may act as the preferred nucleation site for crystallization of the amorphous alloy. The primary crystals, that is, $\alpha-Fe$ may be easily oxidized during sliding friction experiments and transform into $\alpha-Fe_2O_3$.

Thus, a strong interaction between transition metals and metalloids such as boron results in strong segregation and provides preferential transition metalloid clustering [10,11] in the bulk of the amorphous alloy during the sliding friction process. A highly strained amorphous alloy tends to promote clustering of the amorphous alloy long before the surface may otherwise be ready for such clustering. The extent of segregation of metalloids to clusters and/or crystallites is controlled by strain and this may control the strength of the alloys, as well as friction and wear properties of the alloys.

4

Temperature Effects

Typical examples of the structure are shown in Fig. 10 for the amorphous alloy foils after heating to 350° and 430° C for 20 min in ultra-high vacuum. The structure of foil heated to 350° C is similar to that of the as-received foil already shown in Fig. 2. In the structure of the foil that had been heated to 430° C, which is the so-called crystallization temperature for this particular $Fe_{67}Co_{18}B_{14}Si_1$ foil, the black spots are slightly larger than those shown in Figs. 2 and 10(a). The diffused honeycomb-shaped structure formed by dark grey bands is enriched and indicates sub-division of amorphous alloy structure as a result of decomposition and separation of amorphous phase. That is, segregation of constituents and preferential clustering are taking place at this temperature. The electron diffraction pattern also indicates the presence of an extra outer ring related to clustering or crystallinity.

Figure 11 presents microstructures of the foils heated to 500° and 750° C. They reveal two kinds of extremely fine-grained crystals: a dark grain and a light grain. Energy dispersive X-ray analysis indicated that the light grains contained about 20 times more silicon than the dark grains [3]. The dark grains contained more iron and Fe-B alloy. The transmission electron diffraction patterns for both the dark and light grains contained diffraction spots and Kikuchi lines indicating single-crystal structure [3]. The crystallized grain size was 0.7 μm at 500° C and to 1.4 μm at 750° C. Thus, the micro-structure of the amorphous alloy changes discontinuously and drastically during the amorphous to crystalline transition. The amorphous phase separates into two crystalline phases.

Temperature effects lead to drastic changes in surface chemistry of the amorphous alloys as analyzed by XPS and not only above the crystallization temperature, but below it as well. These changes are due to segregation and diffusion of constituents, especially of metalloids such as boron and silicon.

A typical example of the XPS spectra of B_{1s} and Si_{2p} peaks obtained on $Fe_{67}Co_{18}B_{14}Si_1$ foil surface is presented in Fig. 12.

The B_{1s} photoelectron peaks of the as-received specimen indicate the presence of boric oxide as well as Fe_2B and CoB. The spectrum of the surface that had been argon sputter cleaned for 30 and 60 min reveals large peaks for boron and its alloys as well as very small boric oxide peaks.

The spectra for the foils that had been heated to 750° C clearly indicate that the foil surfaces were again contaminated with boric oxide at 350° C and boron nitride at 750° C that had migrated from the bulk of the foil specimens. The foil surfaces heated at 500° C were also contaminated with boron nitride and were the same as that for the heated surface at 750° C.

The Si_{2p} photoelectron peaks of the as-received surface reveal silicides. Even the spectrum of the surface that had been argon sputter cleaned for 60 min reveals silicides as well as silicon oxide on the surface. The foil that had been heated to 350° C was contaminated with silicon oxide that had migrated from the bulk of the foil specimens. The foil heated at 750° C contains a small amount of silicon dioxide on the surface compared to that heated at 350° C.

The Fe_{2p} photoelectron peaks of the $Fe_{67}Co_{18}B_{14}Si_1$ foil heated to 350° and 750° C are almost the same as that for the argon-sputter-cleaned surface shown in Fig. 3.

The Co_{2p} photoelectron peaks of the as-received $Fe_{67}Co_{18}B_{14}Si_1$ foil indicated cobalt oxide. The spectra for the surfaces that had been argon-sputter-cleaned and heated to 350° and 750° C revealed cobalt and its alloy peaks. The cobalt oxide peak was negligible [3].

Table III summarizes the surface conditions of the foils analyzed by XPS. Generally, the XPS results indicate that the surfaces of the as-received foils consisted of a layer of oxides of alloying elements as well as a simple, adsorbed film of oxygen and carbon. The argon sputter cleaned surface consisted of the alloy and small amounts of oxides and carbides. In addition to nominal element constituents, the surface heated to 350° C contained boric and silicon oxides on $Fe_{67}Co_{18}B_{14}Si_1$ and $Fe_{81}B_{13.5}Si_{3.5}C_2$ alloys, and boric oxides on $Fe_{81}Ni_{38}Mo_4B_{18}$ alloys as well as small amounts of carbides that had segregated and migrated from the bulk of the foils. The surface heated to 750° C contained boron nitride that had also migrated from the bulk of the foils as well as small amounts of oxides.

Thus, in situ examinations of the surface chemistry in the heating stage gives valuable information on the behavior of surface segregation and decomposition. The segregation and migration of compounds such as boric oxide and nitride influence the friction behavior of amorphous alloys.

Sliding friction experiments were conducted with aluminum oxide in contact with amorphous alloys in vacuum at temperatures to 750° C. Friction-force traces resulting

from such sliding were generally character-ized by fluctuating behavior with evidence of stick-slip [3]. The coefficient of fric-tion as a function of the sliding temperature of the foil specimen is indicated in Fig. 13. The aluminum oxide rider was sputter cleaned with argon ions at room temperature. The foil specimen was also sputter cleaned with argon ions in the vacuum system and then heated from room temperature to 750° C. The coefficient of friction increased with in-creasing temperature from room to 350° C. The increase in friction is due to an in-crease in the adhesion resulting from segre-gation of boric oxides and silicon oxides to the foil surface as described earlier. Gen-erally, the presence of oxygen does strength-en the metal-ceramic material (such as SiC) contacts and increases the friction [12].

Above 500° C the coefficient of friction decreased dramatically. The rapid decrease in friction above 500° C correlated with the segregation of boron nitride on the foil sur-face, as already discussed and shown in Fig. 12(c). It is also interesting in Fig. 13 that there is a considerable differ-ence in the friction measured for the varia-tions in alloy chemistry.

6. CONCLUSION

The following conclusions are drawn from the presented data:

(1) Amorphous alloys are not completely amorphous, but contain extremely small clus-ters or crystallites (nuclei) of approximate-ly a few nanometers (up to 4 nm) in size.

(2) Surface oxide layers present on the amorphous alloys are stable and very effective in providing low friction and a protective film against wear in an air atmosphere.

(3) Plastic flow occurs on an amorphous alloy surface with sliding. Multiple slip bands due to shear deformation are observed on the sides of the wear track.

(4) Enhanced clustering and crystal-lizing of amorphous alloys occur during the sliding process at a low sliding velocity where the temperature rise is negligible. Clusters or crystallites with sizes to 150 nm and diffused honeycomb-shaped structure formed by dark grey bands are produced on the wear surface of the amorphous alloy.

(5) Temperature effects lead to drastic changes in surface chemistry and friction behavior of the amorphous alloys in the range of room temperature to 750° C. Contaminants can come from the bulk of the material to the surface upon heating and impart to the sur-face boric oxide and/or silicon oxide at 350° C and boron nitride above 500° C. The

segregation of contaminants is responsible for the friction behavior. The coefficient of friction increases with increasing tem-perature to 350° C in vacuum. The increase in friction is due to an increase in adhesion resulting from surface segregation of boric oxide and/or silicon oxide to the surface of the foil.

Above 500° C the coefficient of friction decreased rapidly. The decrease correlates with the segregation of boron nitride to the surface.

(6) The microstructure of amorphous alloy changes discontinuously from the amor-phous phase to the multi-crystalline phases during the crystallization process.

REFERENCES

[1] DeCristofaro, N., and Henschel, C., Weld. J. (Miami), Vol. 5, no. 7, p. 33, (1978)

[2] Miyoshi, K. and Buckley, D. H., "Friction and Surface Chemistry of Some Ferrous-Base Metallic Glasses," NASA TP-1991, (1982)

[3] Miyoshi, K. and Buckley, D. H., "Surface Chemistry, Microstructure, and Friction Properties of Some Ferrous-Base Metallic Glasses at Temperatures to 750° C," NASA TP-2006, (1982)

[4] Miyoshi, K. and Buckley, D. H., "Sliding Induced Crystallization of Metallic Glass," NASA TP-2140, (1983)

[5] Amuzu, J. K. A., J. Phys. D, Vol. 13, p. L127 (1980)

[6] Zum Gahr, K. H. and Nöcker, H., Metall. (Berlin), Vol. 35, No. 10 p. 988, (1980)

[7] Ozawa, K., Wakasugi, H. and Tanaka, K., IEEE Transactions on Magnetics, Vol. Mag.-20, No. 2, p. 425, (1984)

[8] Miyoshi, K. and Buckley, D. H.:, "Friction and Wear of Some Ferrous-Base Metallic Glasses," ASLE Preprint No. 83-LC-5A3, (1983); NASA TM-83067, (1983)

[9] Barquins, M., Kennel, M. and Courtel, R., Wear, Vol. 11, p. 87, (1968)

[10] Köster, U. and Herold, U., "Glassy Metals I," edited by H. J. Güntherodt and H. Beck, Springer-Verlag, P. 225, (1981)

[11] Polk, D. E. and Giessen, B. C., Metallic Glasess, American Society for Metals, p. 1, (1978)

[12] Miyoshi, K. and Buckley, D. H., "Effect of Oxygen and Nitrogen Interactions on Friction of Single-Crystal Silicon Carbide," NASA TP-1265 (1978)

TABLE I. – PROPERTIES OF METALLIC GLASSES

Nominal alloy composition, wt %	Crystallization temperature, °C	Density, g/cm^3	Hardness, GPa	Ultimate tensile strength, GPa	Bend ductility,[a] ϵ
$Fe_{67}Co_{18}B_{14}Si_1$	430	7.56	10	1.5	1
$Fe_{81}B_{13.5}Si_{3.5}C_2$	480	7.3	10.3	0.7	9×10^{-3}
$Fe_{40}Ni_{38}Mo_4B_{18}$	410	8.02	10.5	1.38	1

[a] $\epsilon = t(d-t)$, where t is ribbon thickness and d is micrometer spacing at bend fracture.

TABLE II. – COMPOSITION OF ARGON–SPUTTER–CLEANED
SURFACE LAYER OF AMORPHOUS ALLOYS

Nominal bulk composition		Composition on surface,
wt %[a]	at. %	at. %[b]
$Fe_{67}Co_{18}B_{14}Si_1$	$Fe_{42}Co_{11}B_{46}Si_1$	$Fe_{49}Co_{14}B_{17}Si_6C_9O_5$
$Fe_{81}B_{13.5}Si_{3.5}C_2$	$Fe_{48}B_{42}Si_4C_6$	$Fe_{43}B_{15}Si_8C_{21}O_{14}$
$Fe_{40}Ni_{38}Mo_4B_{18}$	$Fe_{23}Ni_{21}Mo_1B_{55}$	$Fe_{18}Ni_{28}Mo_1B_{24}C_{15}O_{14}$

[a] Manufacturer's analysis.
[b] Relative concentrations of the various constituents
were determined using peak area sensitivity factors
and peak area.

TABLE III. – SURFACE OF AMORPHOUS ALLOYS

Alloy composition	Surface			
	As received	Argon sputter cleaned	Heated to 350° C	Heated to 750° C
$Fe_{67}Co_{18}B_{14}Si_1$	Oxides of Fe, Co, B, Si, and C Adsorbed film of oxygen and carbon	Alloy Small amount of oxides and carbides	Alloy Boric oxides and silicon oxides migrated from bulk Small amount of carbides	Alloy Boron nitride migrated from bulk Very small amount of boric oxides and silicon oxides
$Fe_{81}B_{13.5}Si_{3.5}C_2$	Oxides of Fe, B, Si, and C Adsorbed film of oxygen and carbon	Alloy Small amount of oxides and carbides	Alloy Boric oxides and silicon oxides migrated from bulk Small amount of carbides	Alloy Boron nitride migrated from bulk Very small amount of boric oxides and silicon oxides
$Fe_{40}Ni_{38}Mo_4B_{18}$	Oxides of Fe, B, Ni, Mo, and B Adsorbed film of oxygen and carbon	Alloy Small amount of oxides and carbides	Alloy Boric oxides migrated from bulk Small amount of carbides	Alloy Boron nitride migrated from bulk Very small amount of boric oxides

X-RAY SOURCE

ION SPUTTER GUN

CAROUSEL
SPECIMEN
MOUNT
FLAT
SPECIMEN
HOLDER

ANALYZER

FLAT
SPECIMEN

INSULATOR

LOAD

STRAIN GAGE

THERMOCOUPLE

FRICTION FORCE

ADHESION FORCE

POWER FOR
HEATING

TRANSLATIONAL MOTION

DIRECTION OF SLIDING

TANTALUM SHEET

PIN SPECIMEN
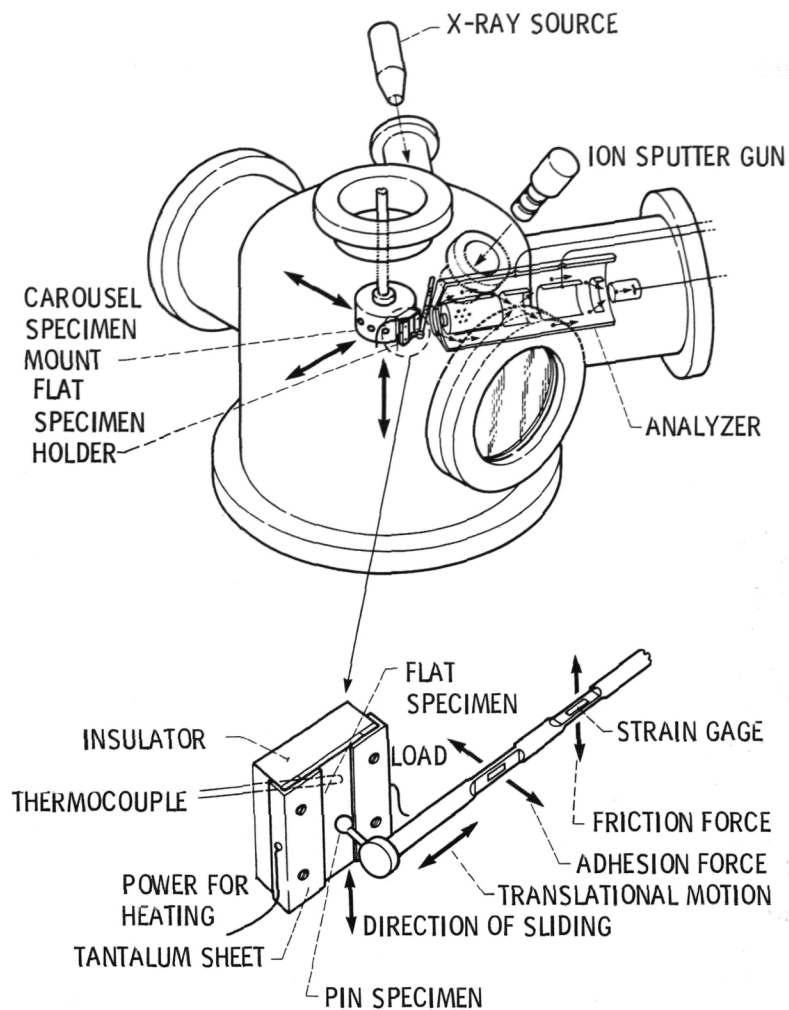
(a) Ultra high-vacuum friction and wear apparatus.

Figure 1. – Friction and wear apparatuses.

FLAT WITH FOIL SPECIMEN
MOUNTED THEREON

LOAD

STRAIN
GAGES

RIDER

DRIVE
MOTOR

MOTION

PIN
FLAT
(FOIL)

GEARBOX
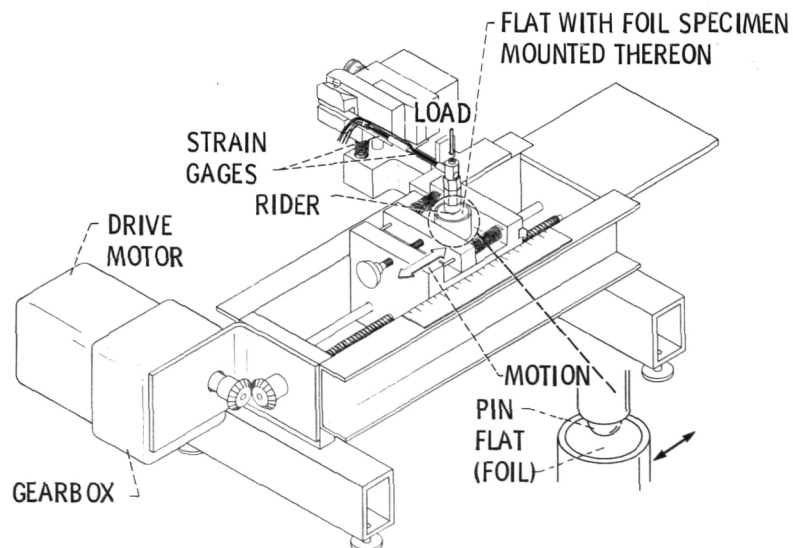
(b) Friction and wear apparatus used in argon and in laboratory air.

Figure 1. – Concluded.

BLACK SPOT

0.02μm
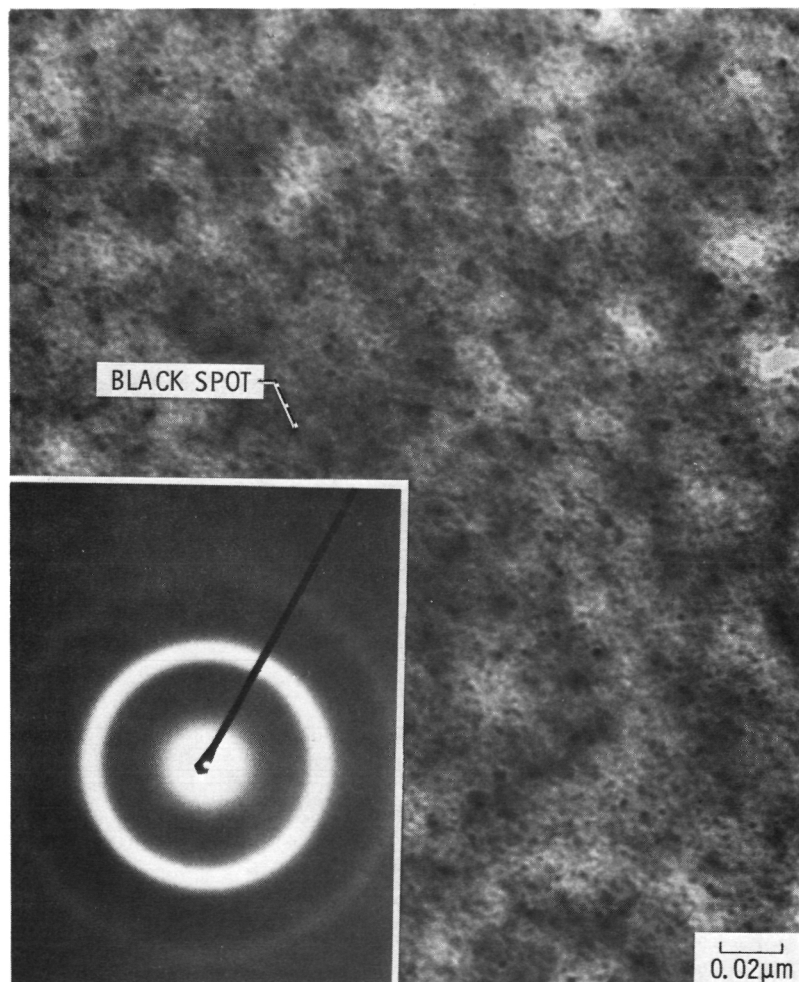
Figure 2. – Typical microstructure and electron diffraction pattern of an amorphous alloy ($Fe_{67}Co_{18}B_{14}Si_1$).

IRON OXIDES

Fe$_{2p1/2}$ Fe$_{2p3/2}$

AT ROOM TEMPERATURE
BEFORE CLEANING

Fe

AFTER ARGON SPUTTER
CLEANING FOR 2 min

Fe

AFTER ARGON SPUTTER
CLEANING FOR 4 min

AFTER ARGON SPUTTER
CLEANING FOR 60 min

INTENSITY

740   730   720   710   700   690
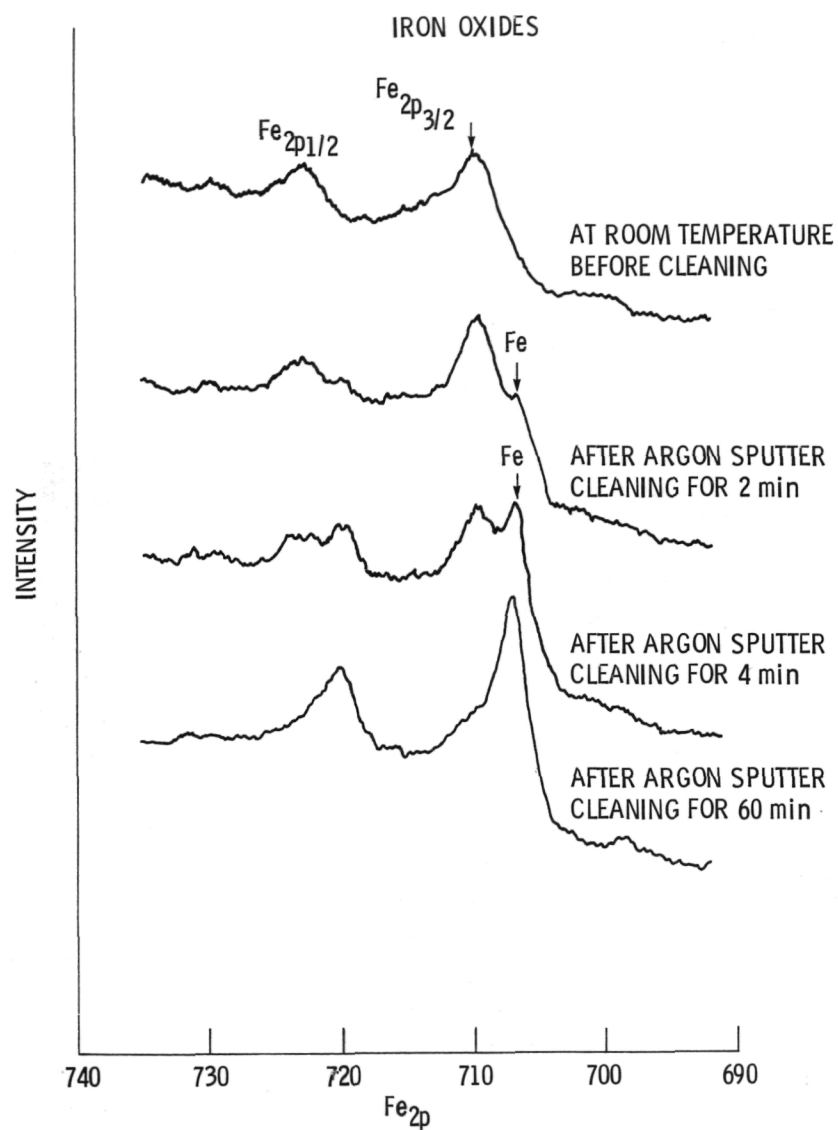
Fe$_{2p}$

Figure 3. – Fe$_{2p}$ XPS peaks on Fe$_{67}$Co$_{18}$B$_{14}$Si$_1$ surface.
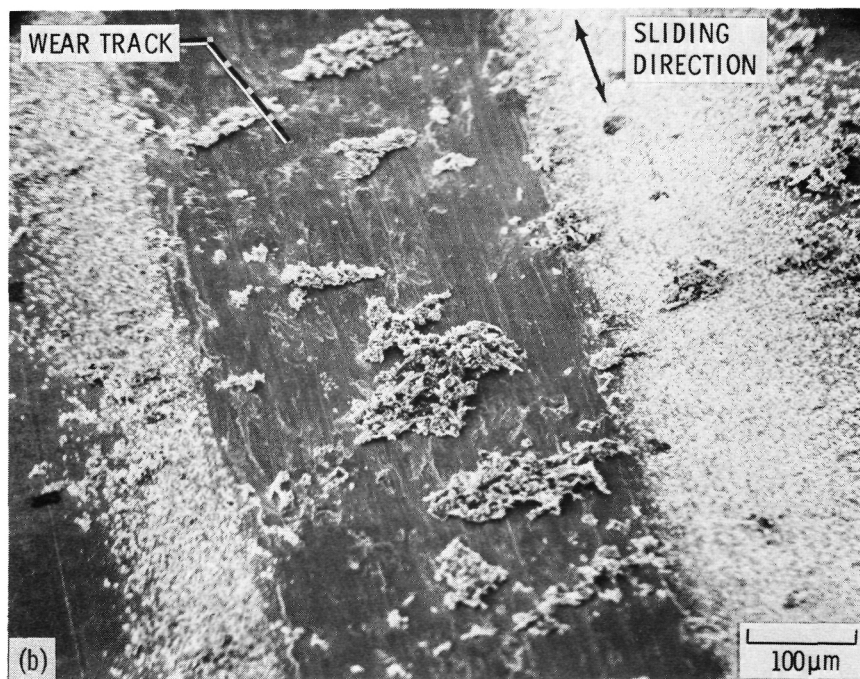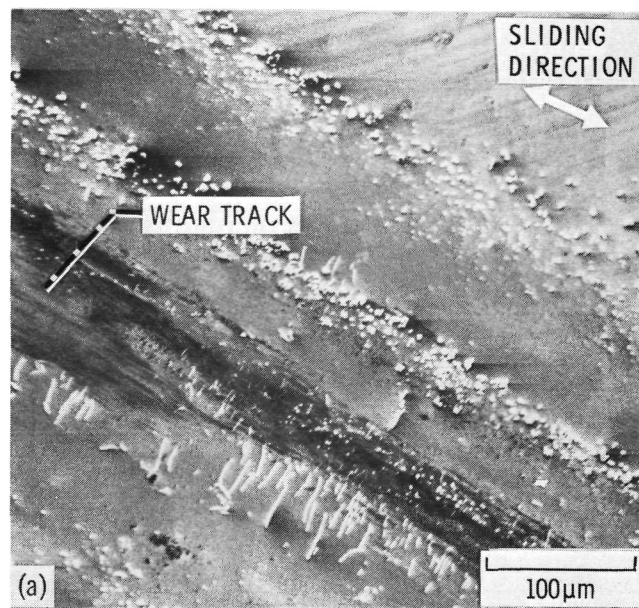
(a) $Fe_{67}Co_{18}B_{14}Si_1$.

(b) 304 stainless steel.

Figure 4. - Scanning electron micrographs of wear track on $Fe_{67}Co_{18}B_{14}Si_1$ amorphous alloy and wear track on 304 stainless steel. Pin, 3.2 millimeters diameter aluminum oxide sphere; load, 2.5 newtons; sliding velocity, 1.5 millimeters per second; sliding distance, 27 meters; room temperature; laboratory air atmosphere; relative humidity, 40%.
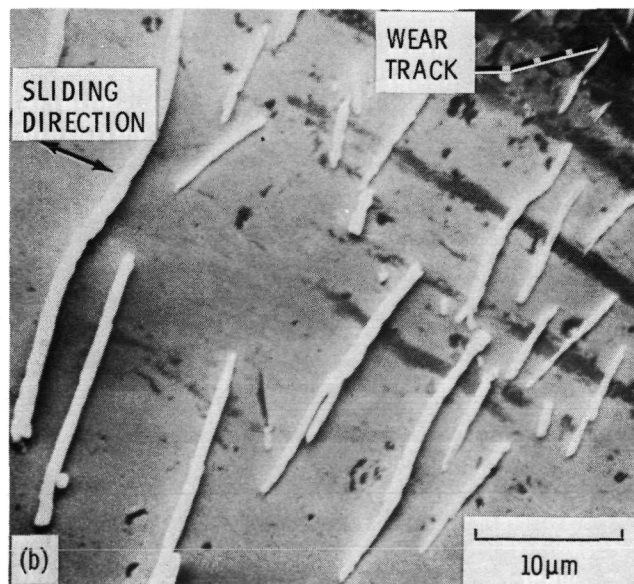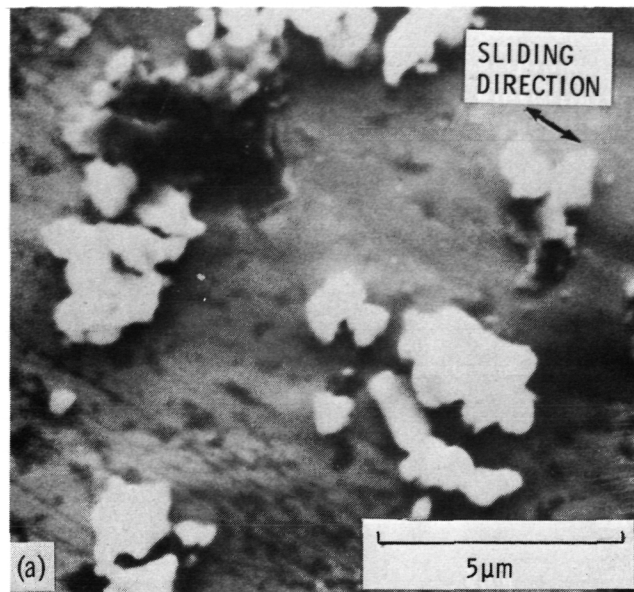
(a) Powdery debris on the wear track.

(b) Whiskery debris on the side of wear track.

Figure 5. - Scanning electron micrographs of powdery and whiskery wear debris particles produced on $Fe_{67}Co_{18}B_{14}Si_1$ amorphous alloy. Pin, 3.2 millimeters diameter aluminum oxide sphere; sliding velocity, 1.5 millimeters per second; load, 2.5 newtons; sliding distance, 27 meters; room temperature; laboratory air atmosphere; relative humidity, 40%.
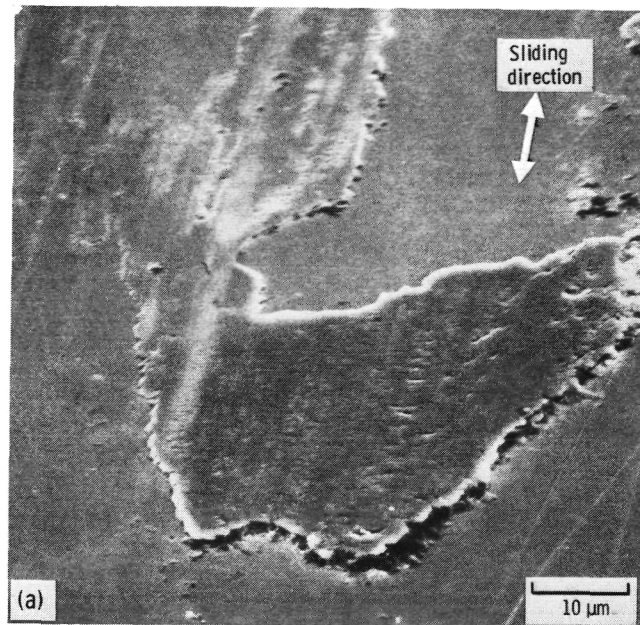
(a) Wear track.
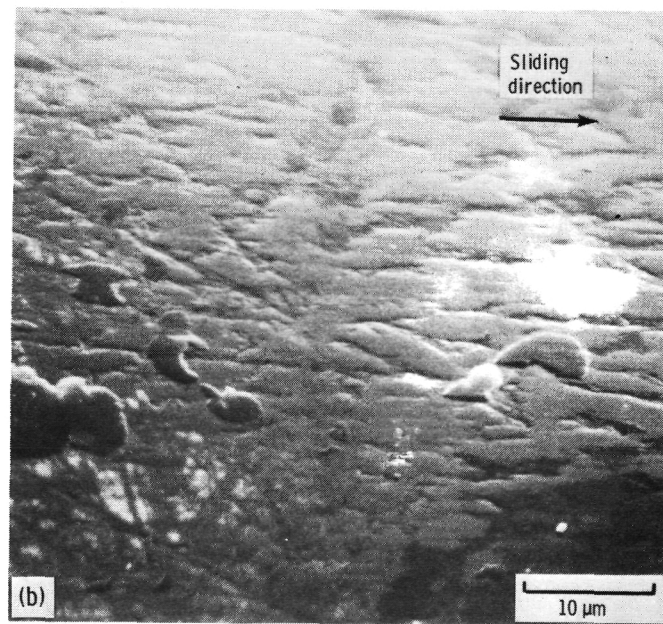
(b) Wear scar.

Figure 6. – Scanning electron micrographs of wear track on $Fe_{67}Co_{18}B_{14}Si_1$ amorphous alloy and wear scar on aluminum oxide rider sliding on $Fe_{67}Co_{18}B_{14}Si_1$ amorphous alloy surface. Rider, 3. 2-millimeter-diameter aluminum oxide sphere; load, 2. 5 newtons; sliding velocity, 1. 5 millimeters per second; sliding time, 5 hours; sliding distance, 27 meters; room temperature; laboratory air atmosphere.

(a) Wear damage.
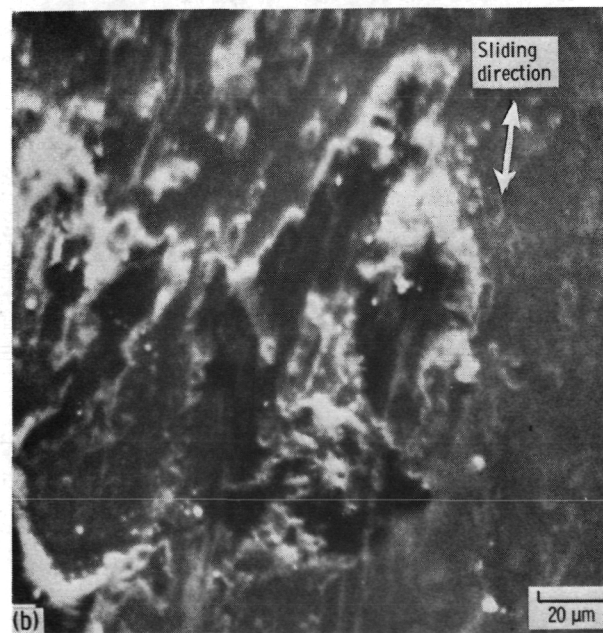
(b) Back-transferred wear debris.

Figure 7. - Scanning electron micrographs of wear track on $Fe_{67}Co_{18}B_{14}Si_1$ amorphous alloy at sliding period of 150 hours. Rider, 3.2-millimeter-diameter aluminum oxide sphere; load, 2.5 newtons; sliding velocity, 1.5 milli-meters per second; sliding time, 150 hours; sliding distance, 810 meters; room temperature; laboratory air atmosphere.
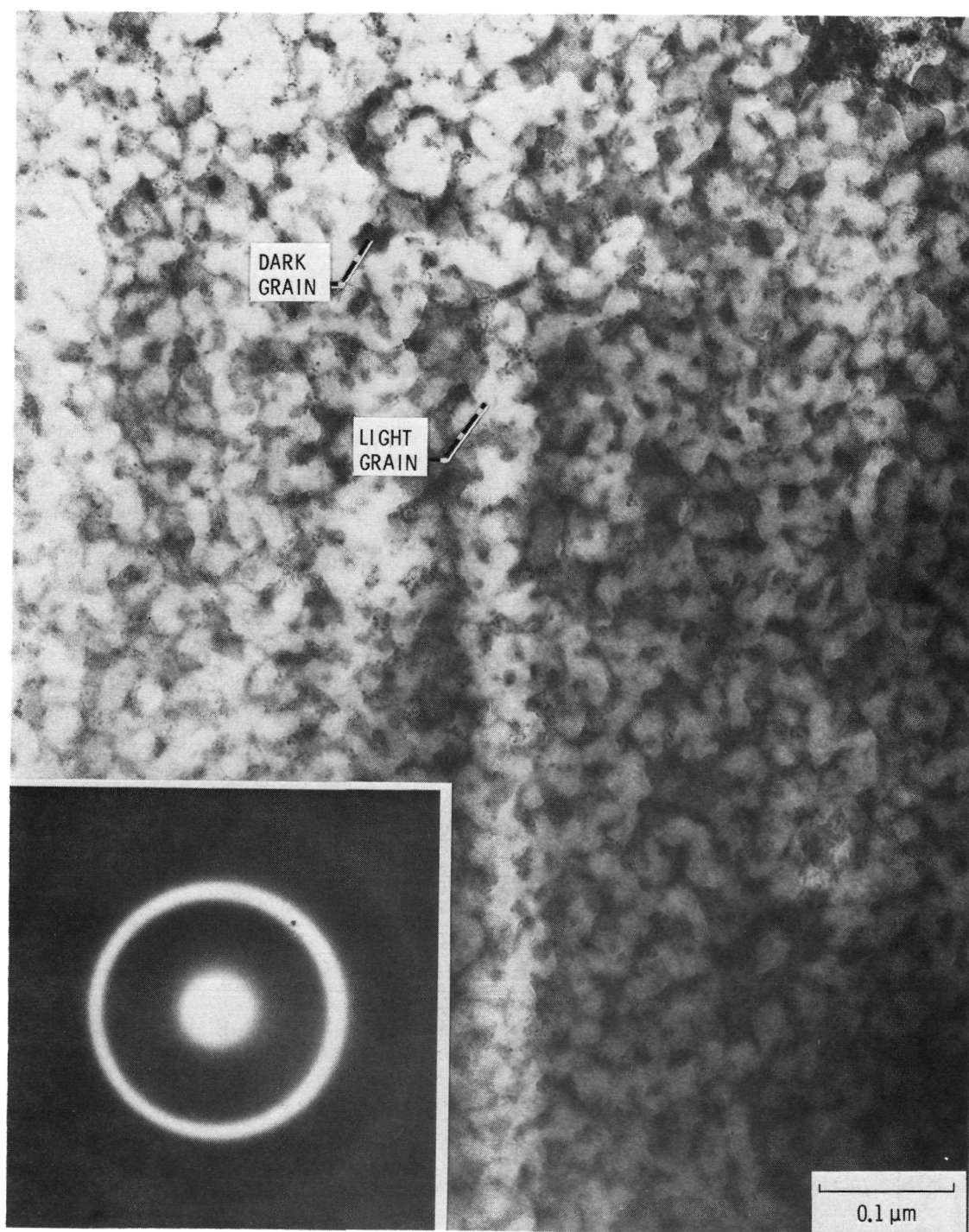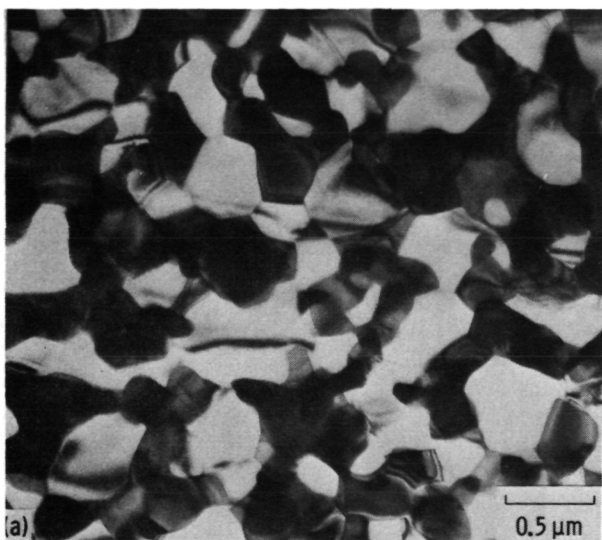
Figure 8. - Typical microstructure and electron diffraction patterns of wear surface of metallic glass ($Fe_{67}Co_{18}B_{14}Si_1$). Rider, 3.2 - millimeter-diameter aluminum oxide sphere; load, 2.5 newtons; sliding velocity, 1.5 millimeters per second; sliding time, 150 hours; sliding distance, 810 meters; room temperature; laboratory air atmosphere.

(a) Bright field.
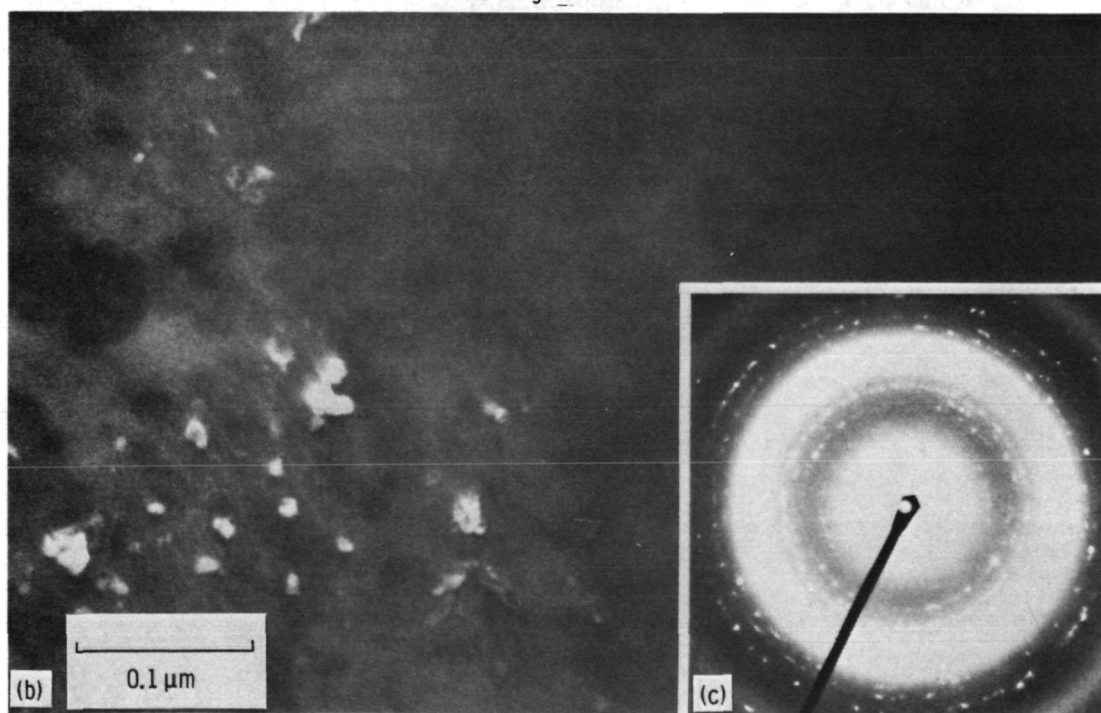
(b) Dark field.

(c) Diffraction pattern.

Figure 9. - Microstructure and electron diffraction patterns of wear surface of metallic glass ($Fe_{67}Co_{18}B_{14}Si_1$). Rider, 3.2-millimeter-diameter aluminum oxide sphere; load, 2.5 newtons; sliding velocity, 1.5 millimeters per second; sliding time, 150 hours; sliding distance, 810 meters; room temperature; laboratory air atmosphere.
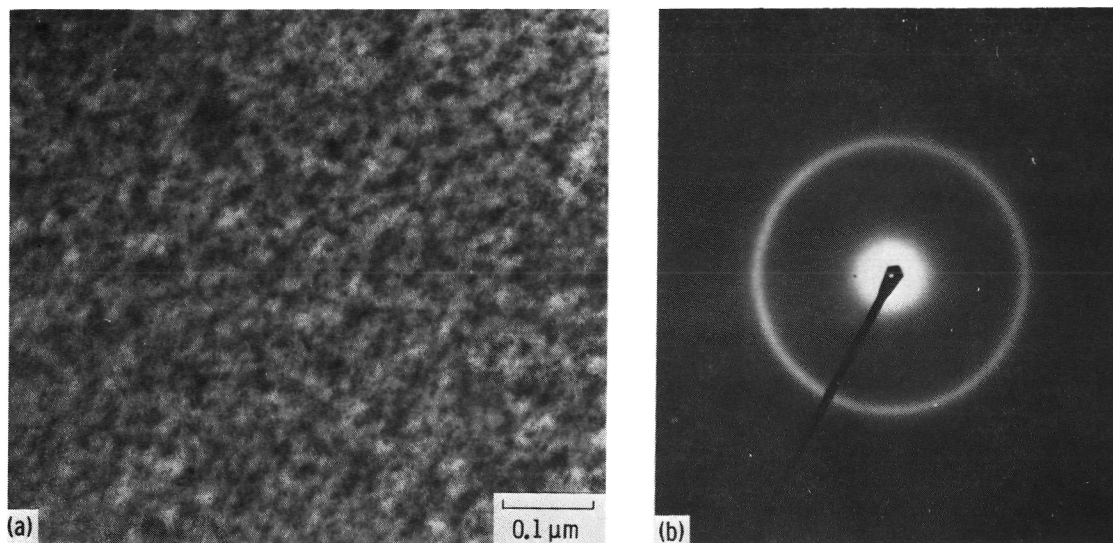
Metallic glass heated to 350° C: (a) microstructure and (b) diffraction pattern.
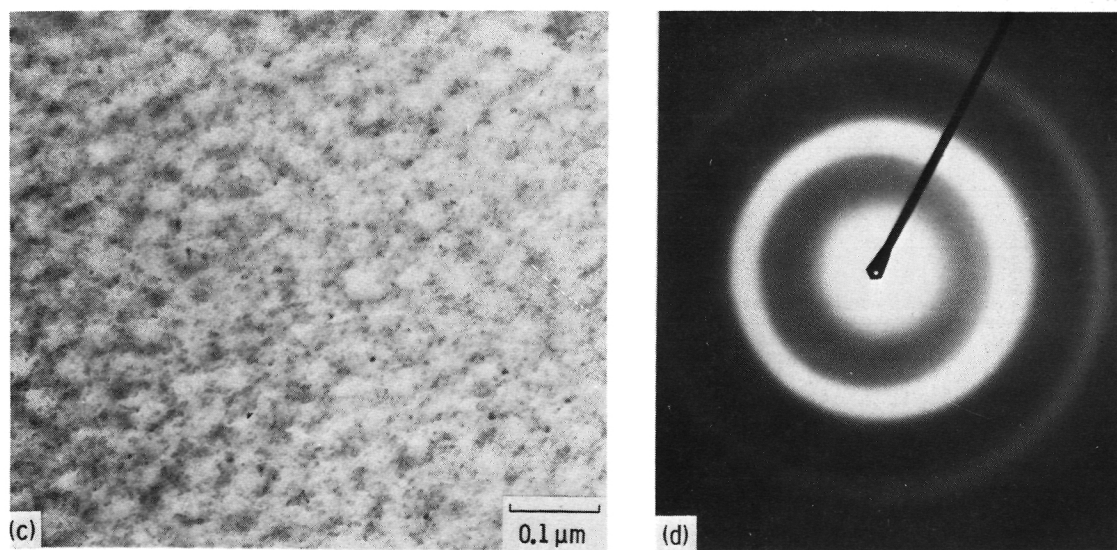
Metallic glass heated to 430° C: (c) microstructure and (d) diffraction pattern.

Figure 10. – Microstructure and electron diffraction pattern of an amorphous alloy $(Fe_{67}Co_{18}B_{14}Si_1)$ heated to 350° C and 430° C in vacuum (10 nPa).

Metallic glass heated to 500° C: (a) microstructure and (b) diffraction pattern.
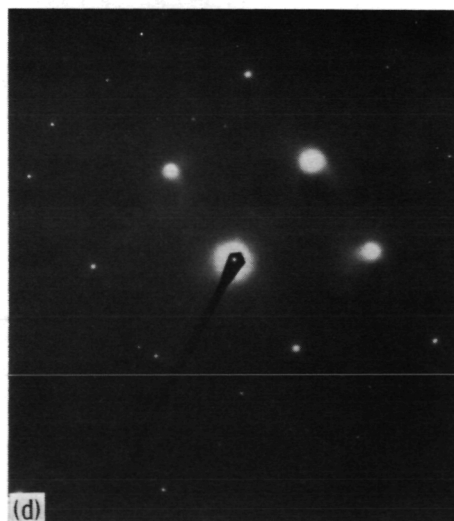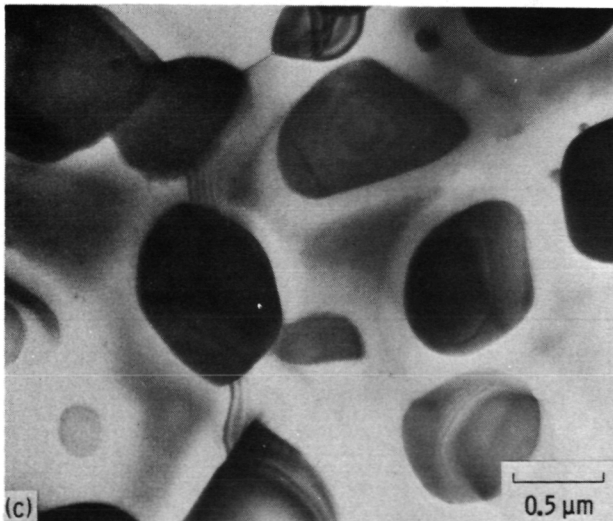
Metallic glass heated to 750° C: (c) microstructure and (d) diffraction pattern.

Figure 11. – Microstructure and electron diffraction pattern of an amorphous alloy $(Fe_{67}Co_{18}B_{14}Si_1)$ heated to 500° C and 750° C in vacuum (10 nPa).
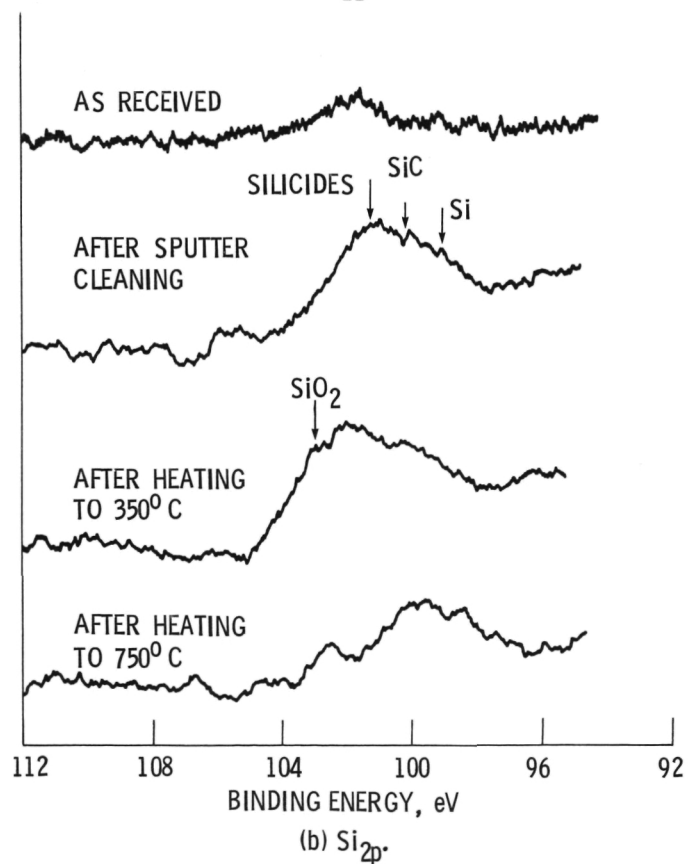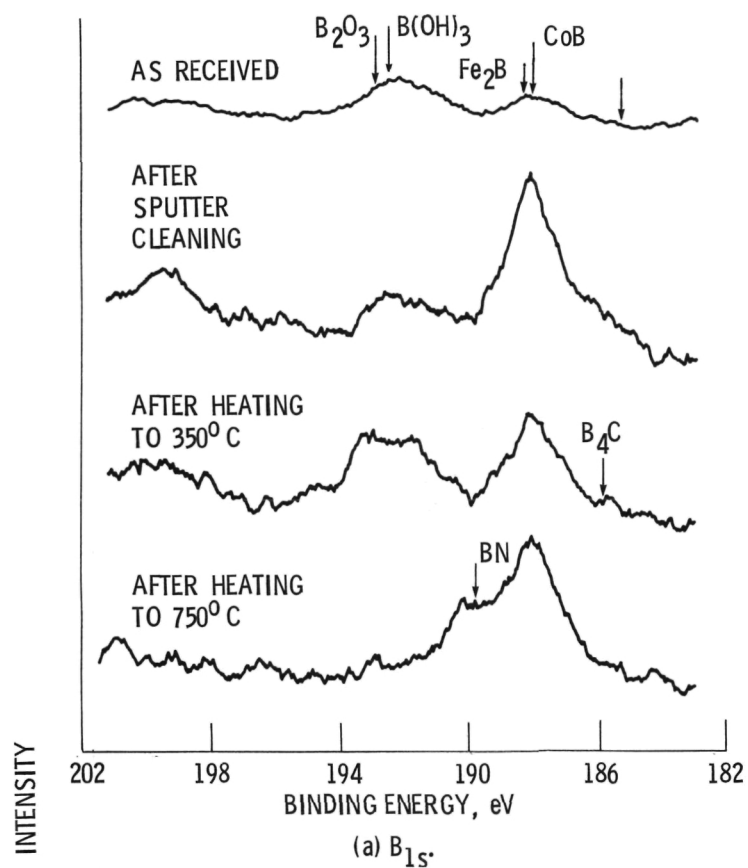
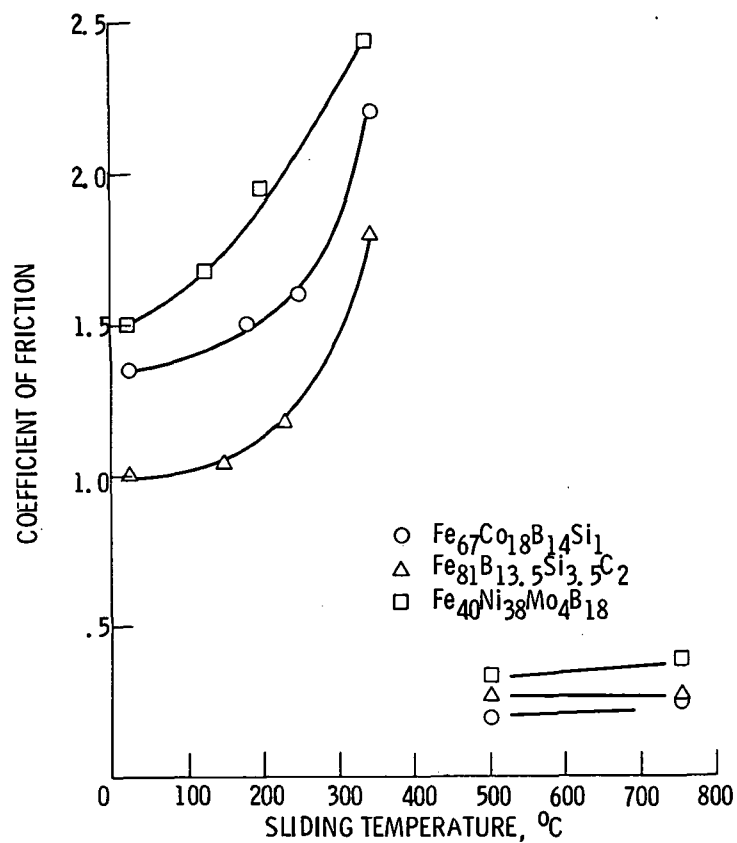Figure 12. - Representative B_{1s} and Si_{2p} XPS peaks on $Fe_{67}Co_{18}B_{14}Si_1$ surface.

Figure 13. - Coefficient of friction as a function of temperature for aluminum oxide sliding on $Fe_{67}Co_{18}B14$ Si_1, $Fe_{81}B_{13.5}Si_{3.5}C_2$, and $Fe_{40}Ni_{38}Mo_4B_{18}$ in vacuum. Normal load, 0.2 N; sliding velocity, 3 mm/min ; vacuum, 10 nPa.

1. Report No. NASA TM-83762	2. Government Accession No.	3. Recipient's Catalog No.
4. Title and Subtitle Microstructure and Surface Chemistry of Amorphous Alloys Important to Their Friction and Wear Behavior		5. Report Date
		6. Performing Organization Code 506-53-1B
7. Author(s) Kazuhisa Miyoshi and Donald H. Buckley		8. Performing Organization Report No. E-2213
		10. Work Unit No.
9. Performing Organization Name and Address National Aeronautics and Space Administration Lewis Research Center Cleveland, Ohio 44135		11. Contract or Grant No.
		13. Type of Report and Period Covered Technical Memorandum
12. Sponsoring Agency Name and Address National Aeronautics and Space Administration Washington, D.C. 20546		14. Sponsoring Agency Code

15. Supplementary Notes

Prepared for the 1985 International Tribology Conference sponsored by the Japan Society of Lubrication, Tokyo, Japan, July 8-10, 1985.

16. Abstract

An investigation was conducted to examine the microstructure and surface chemistry of amorphous alloys, and their effects on tribological behavior. The results indicate that the surface oxide layers present on amorphous alloys are effective in providing low friction and a protective film against wear in air. Clustering and crystallization in amorphous alloys can be enhanced as a result of plastic flow during the sliding process at a low sliding velocity, at room temperature. Clusters or crystallites with sizes to 150 nm and a diffused honeycomb-shaped structure are produced on the wear surface. Temperature effects lead to drastic changes in surface chemistry and friction behavior of the alloys at temperatures to 750° C. Contaminants can come from the bulk of the alloys to the surface upon heating and impart to the surface oxides at 350° C and boron nitride above 500° C. The oxides increase friction while the boron nitride reduces friction drastically in vacuum.

17. Key Words (Suggested by Author(s)) Adhesion; Friction; Wear; Amorphous alloy; Metallic glass	18. Distribution Statement Unclassified - unlimited STAR Category 17		
19. Security Classif. (of this report) Unclassified	20. Security Classif. (of this page) Unclassified	21. No. of pages	22. Price*

SPECIAL FOURTH CLASS MAIL
BOOK

NASA

POSTMASTER: If Undeliverable (Section 158
Postal Manual) Do Not Return